Estuarine, Coastal and Shelf Science 200 (2018) 81–90

Contents lists available at ScienceDirect

Estuarine, Coastal and Shelf Science

journal homepage: www.elsevier.com/locate/ecss

Simulation-based investigation of the generality of Lyzenga's multispectral bathymetry formula in Case-1 coral reef water

Masita Dwi Mandini Manessa [a, b, *], Ariyo Kanno [c], Tatsuyuki Sagawa [d], Masahiko Sekine [c], Nurjannah Nurdin [e]

[a] Center for Remote Sensing and Ocean Science (CReSOS), Udayana University, Denpasar, Bali, Indonesia
[b] Graduate School of Science and Engineering, Yamaguchi University, Ube, Japan
[c] Graduate School of Sciences and Technology for Innovation, Yamaguchi University, Ube, Japan
[d] Remote Sensing Technology Center of Japan, Tokyo, Japan
[e] Marine Science Department, Hasanuddin University, Makassar, Indonesia

ARTICLE INFO

Article history:
Received 21 April 2017
Received in revised form
10 September 2017
Accepted 16 October 2017
Available online 19 October 2017

Keywords:
Bathymetry
Case-1 water
Coral reefs
Lyzenga
Multispectral scanner
Simulation

ABSTRACT

Lyzenga's multispectral bathymetry formula has attracted considerable interest due to its simplicity. However, there has been little discussion of the effect that variation in optical conditions and bottom types—which commonly appears in coral reef environments—has on this formula's results. The present paper evaluates Lyzenga's multispectral bathymetry formula for a variety of optical conditions and bottom types. A noiseless dataset of above-water remote sensing reflectance from WorldView-2 images over Case-1 shallow coral reef water is simulated using a radiative transfer model. The simulation-based assessment shows that Lyzenga's formula performs robustly, with adequate generality and good accuracy, under a range of conditions. As expected, the influence of bottom type on depth estimation accuracy is far greater than the influence of other optical parameters, i.e., chlorophyll-a concentration and solar zenith angle. Further, based on the simulation dataset, Lyzenga's formula estimates depth when the bottom type is unknown almost as accurately as when the bottom type is known. This study provides a better understanding of Lyzenga's multispectral bathymetry formula under various optical conditions and bottom types.

1. Introduction

For maritime countries, bathymetry data in coastal areas is important for nautical information, coastal area zoning, conservation, and scientific studies. Manual bathymetry survey methods use a boat and single- or multiple-beam echo sounder. This technique is time-consuming and becomes hazardous in coastal areas, especially in coral reefs, creating the need for a safe and practical method for extracting bathymetry information from these areas.

Satellite-derived bathymetry (SDB) is a remote sensing approach for analytically or empirically estimating water depth based on the relationships between image pixel values and corresponding depth measurements. In comparison with analytical approaches, which require knowing the optical properties of the water in the targeted mapping area, empirical approaches are simpler, requiring only measurement data and remote sensing images. Thus, empirical approaches, (e.g., hyperspectral and multispectral optical remote sensing) have become the most commonly applied SDB methods. Optical remote sensing data from multispectral images are most often used because of their availability in archive data, variety of spatial resolution options, low cost, and (most importantly) accuracy (Stumpf et al., 2003; Kanno and Tanaka, 2011; Pacheco et al., 2015; Eugenio et al., 2015; Vinayaraj et al., 2016; Kabiri, 2017). Multispectral SDB is a powerful tool for mapping shallow water; compared with conventional manual survey methods, bathymetry data can be derived more quickly, cheaply, and safely—often at a higher spatial resolution (depending on the spatial resolution of the remote image).

Over the past three decades, several empirical methods for deriving bathymetry data from multispectral imagery have been proposed and investigated (Paredes and Spero, 1983; Lyzenga, 1985; Clark et al., 1987; Spitzer and Dirks, 1987; Philpot, 1989;

* Corresponding author. Geodesy Department, Pakuan University, Bogor 16143, Indonesia..
E-mail addresses: m.manessa@outlook.com, mdm.manessa@gmail.com (M.D.M. Manessa).

https://doi.org/10.1016/j.ecss.2017.10.014
0272-7714/

Jupp, 1988; Stumpf et al., 2003; Leckie et al., 2005; Lyzenga et al., 2006; Daniell, 2008; Su et al., 2008, 2013; Vinayaraj et al., 2016; Manessa et al., 2016a; Kabiri, 2017; Ribeiro et al., 2008). The empirical SDB methods that utilize multispectral data can be categorized into four main techniques: 1) The stratified genetic algorithm (SGA) is an extension of the depth-of-precision (DOP) model proposed by Jupp (1988). 2) Stumpf et al. (2003) proposed a nonlinear inversion model, which was modified by Su et al. (2008) to include automated parameter calibration. 3) In a further modification of the previous method, Su et al. (2013) combined linear and geographically-adaptive inversion models, and Vinayaraj et al. (2016) combined linear and adaptive geographically-weighted regression models. Both groups aimed to handle the effects of geographic variation. 4) The most popular method for use in coral reef environments has been the multiple linear regression (MLR) method developed by Lyzenga et al. (2006) based on previously proposed methods (Paredes and Spero, 1983; Lyzenga, 1985; Clark et al., 1987). Lyzenga MLR has an especially interesting feature: although it began as an empirical method (Lyzenga, 1985; Lyzenga, 1978), Lyzenga et al. (2006), Kanno et al. (2013), and Manessa et al. (2016b) have shown that it can be used analytically to build a depth estimation formula.

The Lyzenga method is based on the simple assumption of a linear relation between water depth and surface reflectance. Combining multiple linearized visible bands (i.e., the logarithm of radiance or reflectance values) and known depth pixels into a linear formula for depth estimation, Lyzenga's multispectral bathymetry model has been used widely and successfully in many applications (Liceaga-Correa and Euan-Avila, 2002; Flener et al., 2012; Yuzugullu and Aksoy, 2014; Pacheco et al., 2015; Manessa et al., 2016a; Vinayaraj et al., 2016). Multiple combinations of bands are applied to reduce the negative effects of optical conditions, such as bottom type and water quality, on the estimated depth values. Despite this mitigating step, Lyzenga et al. (2006) posited that this method is only effective when the water quality is less heterogeneous and the number of bottom types is less than the number of bands used as input, which is unrealistic, especially in coral reef environments. Therefore, the generality of this method and its robustness under varying conditions (especially bottom types) is still an essential question.

Coral reef environments exhibit a wide range of water quality features and bottom types with unique spectral characteristics and spatial distributions. The goal of this study is to assess the influence of optical conditions and the number of bottom types on the generality of Lyzenga's multispectral bathymetry retrievals in Case-1 shallow coral reef waters. This evaluation is carried out using a simulated WorldView-2 above-water reflectance dataset that combines the spectral properties of several archived coral reef field reflectance measurements, along with various depths and modeled inherent optical properties (IOPs) of Case-1 coral reef water scenarios. The simulated dataset is in line with a variation used by Lee et al. (2013), and Manessa et al. (2016c).

The simulated dataset is used for three analyses: First, Lyzenga's bathymetry formula is tested on a simulated dataset that represents a coral reef environment to determine whether Lyzenga's assumptions were unrealistic (the assumption that the number of bottom types is no more than number of bands is unrealistic for many coral reefs, where bottoms can be covered not only by sand, rocks, and algae but also by various species of corals with a variety of colors). In real-world data, the number of bottom types tends to vary more than water quality. Second, the effect of the quantity of bottom types present at a site is tested, representing the full range of bottom-type diversity that might appear in coral reef environments. Third, Lyzenga's formula is tested for unknown bottom types. Ideally, the pixels with known depth used as input in Lyzenga's bathymetry formula should represent the range of depths and bottom types in the targeted area. However, it difficult to obtain representative input because of the large area and varied bottom types of coral reef environments. Thus, this analysis becomes important for evaluating the performance of Lyzenga's bathymetry formula.

2. Methods

2.1. Simulated worldview-2 dataset

2.1.1. Dataset description

In this study, a simulated dataset is created to represent multispectral images of a shallow coral reef environment. The simulation dataset is built based on several assumptions specific to the conditions of Case-1 coral reef water. First, the water is very clear with no suspended matter. Second, chlorophyll-α concentrations range from 0.02 mg/m^3 to 5 mg/m^3. Third, the sky is often clear, implying that there is no significant noise from clouds, haze, or smoke. Fourth, due to the high resolution of the spatial imagery, there is a short pixel-mixing spectrum. Finally, the water surface is calm, with no wave refraction, white caps, or sun glint.

Moreover, the simulated dataset is based on a zero-noise assumption. Using the radiative transfer model, the above-water remote sensing reflectance is simulated between 400 nm and 700 nm at a 1-nm resolution and rescaled to the spectral response of the WorldView-2 satellite sensor. Although the WorldView-2 sensor has visible bands with sensitivities greater than 700 nm (band 6), most spectral data available for coral reef bottom types are limited to 700 nm. Therefore, band 6 is excluded from further analysis. Herein, “bands” refer to the first five bands of WorldView-2, namely, the coastal blue (band 1), blue (band 2), green (band 3), yellow (band 4), and red (band 5) bands, unless otherwise stated.

As input, Case-1 water conditions are modeled with differing combinations of water depths (henceforth called “real depths”), chlorophyll concentrations, solar zenith angles, and bottom-type reflectances. Water depth is defined as the height of the water column from the top of a bottom-type object to the water's surface. Chlorophyll-a concentration is used as the only indicator for calculating the absorption and backscatter coefficients. The solar zenith angle is the angle between the zenith and the center of the sun's disc. A bottom type is a specific object or species that covers the ocean crust and is submerged. Detailed values for each input parameter are shown in Table 1. The simulated dataset was processed in the R software environment.

2.1.2. Radiative transfer model

The simulated dataset is built using the radiative transfer model for Case-1 water from Lee et al. (1999). The unit of reflectance used is the remote sensing reflectance at nadir-view just above the surface R_{rs}, which is simulated from the subsurface remote-sensing reflectance r_{rs}, separated into two components due to the water column and bottom reflectance:

$$r_{rs} \approx r_{rs}^{dp}\left(1 - e^{-\left[\frac{1}{\cos(\theta_s)}+D_u^C\right]kH}\right) + \frac{\rho}{\pi}e^{-\left[\frac{1}{\cos(\theta_s)}+D_u^B\right]kH} \quad (1)$$

$$R_{rs} \approx 0.5r_{rs}/1 - 1.5r_{rs} \quad (2)$$

where r_{rs}^{dp} is the subsurface reflectance of optically deep water (infinite depth); ρ is the bottom reflectance; θ_s is the subsurface solar zenith angle; D_u^C and D_u^B are the optical path-elongation factors for scattered photons from the water column and the bottom,

Table 1
Optical conditions for the gridded portion of the simulated dataset.

Parameter	Value [units]
Depth	depth = 0.5•n (n = 1, 3, ⋯, 39) [m]
Chlorophyll-a concentration	chl = $0.02*2^{n/2}$ (n = 1, 3, ⋯, 15) [mg/m^3]
Solar zenith angle	sZ = 3•n (n = 0, 3, ⋯, 15) [degrees]
Bottom spectral reflectance	Field spectra (wavelength 400–700 nm) from 164 types of coral, algae, dead coral, seagrass, and substrates from Indonesia, Japan, and Australia. (Bali, Indonesia: Hochberg et al., 2004; Derawan, Indonesia: Nurlidiasari, 2004; Spermonde, Indonesia: Nurjannah Nurdin, personal archive data; Japan: Sagawa et al., 2010, 2012; Australia: Roelfsema and Phinn, 2012.)
Water refractive index	1.334

respectively; k is the attenuation coefficient; and H is the depth.

The radiative transfer equation parameters depend greatly on the optical properties of the water. Further, the optical properties of Case-1 water mainly depend on chlorophyll-a concentration (Lee et al., 1999). The parameters are expressed through the following equations:

$$r_{rs}^{dp} \approx (0.084 + 0.17u(z,\lambda))u(z,\lambda) \tag{3}$$

$$u(z,\lambda) = \frac{b_b(z,\lambda)}{a(z,\lambda) + b_b(\lambda z,\lambda)} \tag{4}$$

$$k(z,\lambda) = a(z,\lambda)b_b(z,\lambda) \tag{5}$$

$$D_u^c(z,\lambda) \approx \sqrt{1.03(1 + 2.4u(z,\lambda))} \tag{6}$$

$$D_u^b(z,\lambda) \approx \sqrt{1.04(1 + 5.4u(z,\lambda))} \tag{7}$$

$$b_b(z,\lambda) = b_w(\lambda) + b_{bp}(z,\lambda) \tag{8}$$

$$a(z,\lambda) = a_w(\lambda) + a_p(z,\lambda) + a_y(z,\lambda) \tag{9}$$

where k is the attenuation coefficient; a is the absorption and backscattering coefficient; a_w, a_p, and a_y are the absorption coefficients for pure sea water, chlorophyll-bearing particles, and covarying yellow matter (i.e., colored dissolved organic matter; CDOM), respectively; and b_w and b_{bp} are the backscattering coefficients for water and suspended particles, respectively. The pure sea water absorption and backscattering constants a_w and b_w are collected from Baker and Smith (1982). The remaining IOP parameters (a_p, a_y, and b_{bp}) are calculated based on several equations available in the literature (see Appendix).

2.1.3. Optical conditions

The simulated dataset is built by combining gridded and random input steps. The gridded step is used to distribute the value of each parameter evenly. Table 1 shows the optical conditions used in the gridded step to create a total of 211,200 combinations. The random step ensures that bottom-type cases included in the random condition are within the range of conditions that commonly appear in coral reef environments. In this step, water depth, chlorophyll-a concentration, and solar zenith angle are set randomly within the realistic range of optical conditions shown in Table 1. The random step also produced 211,200 combinations.

As a quality control measure, simulated just-above-surface reflectances with a bottom contribution of less than 25% are excluded from the analysis, because they are less accurate (Carder et al., 2005). The percentage of bottom contribution is the ratio of the bottom reflectance component of the remote sensing reflectance at nadir-view just above the surface R_{rs} to the remote sensing reflectance at nadir-view just above the surface R_{rs}, expressed in the following equation:

$$\%\ of\ bottom\ contribution = \left(\left(\frac{0.5\left(\frac{\rho}{\pi} e^{-\left[\frac{1}{\cos(\theta_s)} + D_u^B\right] kH}\right)}{1 - 1.5\left(\frac{\rho}{\pi} e^{-\left[\frac{1}{\cos(\theta_s)} + D_u^B\right] kH}\right)} \right) \Big/ R_{rs} \right) \cdot 100 \tag{10}$$

2.2. Lyzenga's multispectral bathymetry model

2.2.1. Theory

In shallow water, the radiance observed by the satellite using a visible-light sensor consists of four components: atmospheric scattering, surface reflection, in-water volume scattering, and bottom reflection, as follows:

$$\begin{aligned} &Radiance\ at\ TOA = Bottom\ Reflection + in-water\ Scattering \\ &\quad + Surface\ Rereflection + Atmospheric\ Scattering \\ &\quad \text{Or, symbolically, as} \\ &L_{TOA} = B + V + S + A \end{aligned} \tag{11}$$

Then, the observed spectral radiance L or reflectance R at the top of the atmosphere (TOA) is a function of wavelength λ and can be expressed as

$$L_{TOA} = \left(V + (B - V)e^{-kh}\right)TE + S + A \tag{12}$$

$$R_{TOA} = \left(V + (B - V)e^{-kh}\right)T + S/E + A/E \tag{13}$$

where V is the in-water volume scattering reflectance at infinite depth, B is the bottom reflectance, k is the effective attenuation coefficient, h is water depth, T is the round-trip transmittance through the atmosphere and water surface, V is the down-welling irradiance at the top of the atmosphere, S is the surface reflection component, and A is the path radiance. Except for h, all the terms in the equations are functions of λ; however, for notational convenience it is omitted.

Lyzenga used a simple algorithm to explain bottom reflectance in relation to water depth and the physical properties of light. Several optical assumptions underlie Lyzenga's method; it assumes no large changes in water quality and that the number of bottom types is less than the number of bands used as input. The estimation formula is an algorithm based on linear regression. Then, Lyzenga (1978) proposed a transformation to approximately

linearize the relationship between the transformed radiances and water depth:

$$X = \log(R_{TOA} - R_{TOA\infty}) \quad (14)$$

At infinite depth, the exponential function (Eq. (13)) is negligible and can be written as

$$R_{TOA\infty} = VT + S/E + A/E \quad (15)$$

Substitute Eqs. (13) and (15) to Eq. (14) to obtain

$$X = \log\left(\left((B - V)e^{-kh}\right)T\right), \quad (16)$$

which can be simplified to

$$\begin{array}{l} X = -kh + log(B - V)T \\ or \\ X = -kh + C \end{array} \quad (17)$$

where C is a term dependent on the bottom reflectance, an apparent reflectance of deep water due to in-water scattering, round-trip transmittance through the atmosphere and water surface, and downwelling irradiance at the top of the atmosphere. For a multispectral image with an m band, the variables X, k and C are defined as

$$X \equiv (X_1 \ldots X_m) \quad (18)$$

$$k \equiv (k_1 \ldots k_m) \quad (19)$$

$$C = (log(B_1 - V_1)T_1 \ldots log(B_m - V_m)m) \quad (20)$$

Lyzenga et al. (2006) proposed a depth algorithm of the form

$$\widehat{h} = \beta_0 + \beta_1 X_1 + \ldots + \beta_M X_M \quad (21)$$

where β_0, β_0, …, β_0 are coefficients estimated by the least-squares method using pixels with known depth. Necessary and sufficient conditions for $\widehat{h}$ in Eq. (21) to satisfy Eq. (20) are as follows:

$$\sum_{i=1}^{M} \beta_i k_i = -1, \ \beta_0 + \sum_{i-1}^{M} C_i \beta_i = 0 \quad (22)$$

If k, V, and T are homogeneous for pixel $\widehat{h}$, there exists a β that satisfies Eq. (22), provided that the number of bottom types is no greater than M. The preceding algebraic explanation of Lyzenga's multispectral bathymetry was adapted from Lyzenga et al. (2006) and Kanno and Tanaka (2011).

To apply this method to WorldView-2 images, we first correct the above-water surface reflectance by subtracting the remote sensing reflectance of deep water:

$$R_{rs}^{cor} i = R_{rsi} - R_{rs}^{dp} i, \quad (23)$$

where i is the specific WorldView-2 band. Second, the corrected surface reflectance is linearized by taking a natural logarithm to yield X_{rsi}:

$$X_{rsi} = log(R_{rs}^{cor} i) \quad (24)$$

Finally, an MLR analysis is conducted with depth h as the dependent variable and the linearized surface reflectance (X_{rsi}) as the independent variable. The complete multispectral bathymetry formula is summarized as follows:

$$\widehat{h} = \beta_0 - \sum_{i=1}^{n} \beta_i (X_{rsi}), \quad (25)$$

where β_0 is the y-offset, β_i is determined by a regression analysis of depth against linearized reflectance, and n is the number of bands.

2.2.2. Data analysis

This empirical model, from Lyzenga et al. (2006), is used to predict shallow-water bathymetry in the simulated dataset. After quality control (Section 2.1.3), the simulation dataset is analyzed to investigate the performance of Lyzenga's multispectral bathymetry model under a wide range of optical condition. This procedure is shown in Fig. 1.

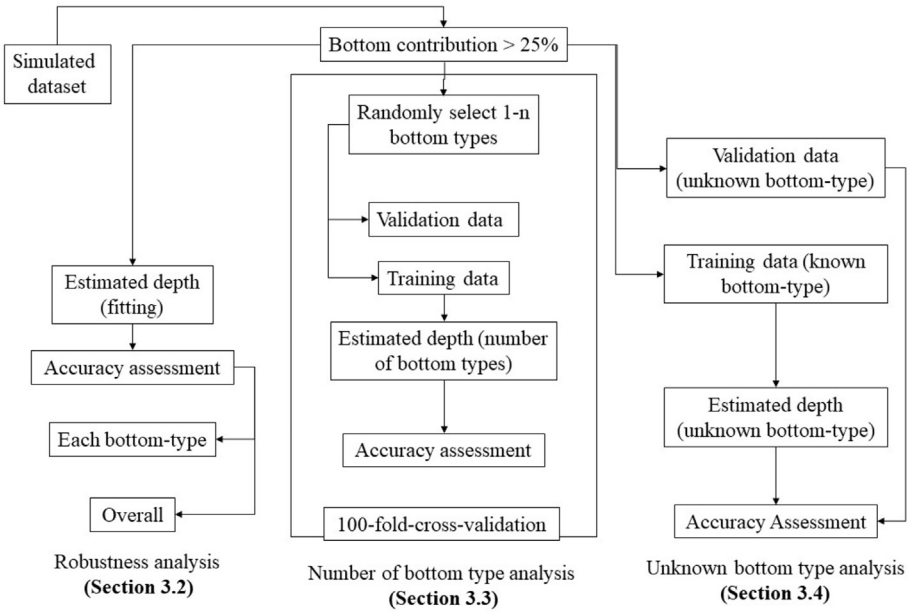

Fig. 1. Workflow for evaluating Lyzenga's bathymetry formula using a simulated dataset.

The workflow used in this study can be described as follows: First, water depths are estimated by applying Lyzenga's multi-spectral bathymetry model—a least-squares analysis, described in Section 2.2.1—to the dataset. The residual r for each data point is the difference between the estimated and true depth values. The relationship between optical conditions and the magnitude of the residuals is then investigated, as described in Section 3.2. Second, to identify the effect of the number of bottom types on depth estimation, 100 possible combinations of bottom types—ranging in number from 1 to the maximum number of archived bottom types—are selected randomly. For each combination, we perform a cross-validation of 100 repeated random subsample validations by randomly splitting the dataset into training and test datasets at a ratio of 9:1 (described in detail in Section 3.3). Last, to test the possibility of predicting depth for unknown bottom types, we perform leave-one-out cross-validation. Each bottom type is excluded from the dataset, then fitting is performed. The excluded bottom type is used as test data (as in Section 3.4). In each section, an accuracy assessment is performed between the depth result from Lyzenga's model (the estimated depth) and depth value of simulated dataset (the real depth).

2.3. Accuracy assessments

Depth estimation accuracy is evaluated using the statistical criteria of the standard deviation σ, coefficient of determination R^2, and root-mean-square (RMS) error, which can be defined as follows:

$$\sigma = \left(\frac{1}{n}\sum_i \left(\widehat{h} - \overline{h}_i\right)^2\right)^{0.5} \tag{26}$$

$$R^2 = 1 - \sum_i \left(h_i - \widehat{h}_i\right)^2 \Big/ \sum_i \left(h_i - \overline{h}\right)^2 \tag{27}$$

$$RMS = \left(\sum_i \left(h_i - \widehat{h}_i\right)^2 / n\right)^{0.5} \tag{28}$$

where h_i and $\widehat{h}_i$ are the real and estimated depths for the i^{th} data item.

3. Results and discussion

3.1. Simulation dataset overview

The simulated dataset, described in Section 2.1, was produced in a tabular format with each row representing a different optical condition and each column representing a variable. The size of the

Table 2
Summary of data removal resulting from quality control requirements and reflectance linearization (Eq. (24)). The initial dataset contained 422,400 rows.

Band	After quality control (>25% of the % bottom contribution)				After linearized reflectance $log(R_{rs}^{cor}i)$			
	Remaining data (rows)	% of initial dataset	Depth range (meters)	No. of bottom types	Remaining data (rows)	% of initial dataset	Depth range (meters)	No. of bottom types
Band 1	253,998	60%	0.5–19.5	164	89,209	22%	0.5–10.5	144
Band 2	305,784	73%	0.5–19.5	164	106,826	25%	0.5–10.5	141
Band 3	344,031	82%	0.5–19.5	164	121,338	28%	0.5–10.5	163
Band 4	189,854	45%	0.5–16.5	164	122,538	29%	0.5–10.5	164
Band 5	124,440	29%	0.5–10.5	164	122,538	29%	0.5–10.5	164
All Bands	122,538	29%	0.5–10.5	164	88,080	21%	0.5–10.5	137

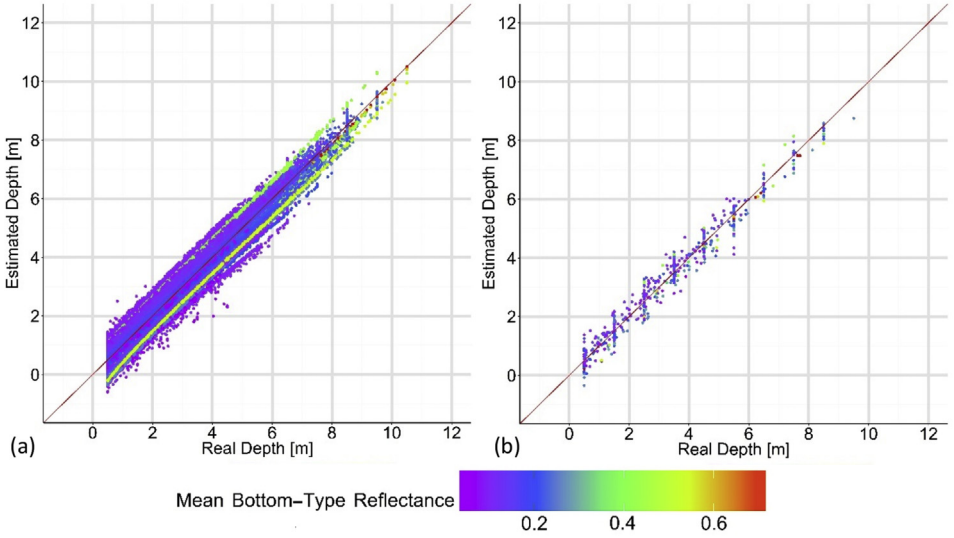

Fig. 2. Scatter plot of fitted values of estimated versus real depth for (a) all data and (b) a subset of 500 randomly selected points. Colors indicate the average spectral reflectance of each bottom type. The red line is y = x, indicating the parity of the model's predictions with real depth. (For interpretation of the references to colour in this figure legend, the reader is referred to the web version of this article.)

Table 3
Statistical summary of the residual data between the estimated and real water depth values.

RMS (m)	Σ	R^2	Mean absolute depth (m)	Maximum absolute depth (m)
0.36	0.36	0.98	0.28	2.94

dataset was 422,400 rows built from gridded and random steps, as described in Section 2.1.3.

Table 2 shows the data removal that occurred following the surface reflectance linearization and quality control steps. The data removal results were spectrally dependent (i.e., different for each band). In the quality control step, low bottom contributions at long wavelengths (band 5) led to the removal of ~70% of the initial data. In this data reduction step, the depth range of the dataset was reduced significantly, from 0.5 to 19.5 m initially to 0.5–10.5 m. These results show that longer wavelength bands and areas of deeper water yielded smaller bottom contributions because of their characteristically high attenuation coefficients. The low bottom contribution of these samples can be explained by the maximum depth of bottom reflectance detectability. As shown in Table 2, after quality control, the maximum depth was less than 10.5 m and data at deeper depths were defined as having a low bottom contribution. Similar results were found by Carder et al. (2005). These findings may also explain the poor bathymetry estimates from actual satellite imagery for depths greater than 10.5 m. However, to confirm this, further investigation is needed. Meanwhile, in the linearized reflectance step, most data removal occurred because of low (<25%) bottom contribution in the short wavelength range (bands 1 and 2), caused by dark object reflectance that was lower than that of deep water. The removal of these spectra affected 141 of the 164 total bottom type objects, as shown in Table 2. This is a known issue in the application of Lyzenga's method (Manessa et al., 2014) in areas with very bright or dark bottom types.

3.2. Performance of Lyzenga's multispectral bathymetry model

3.2.1. Depth estimation accuracy

Fig. 2(a) presents a scatter plot of real and estimated water depths (the result of regression fitting) for all data. For better visual understanding, a subset of 500 data points was randomly selected and is presented in Fig. 2(b). The superiority of Lyzenga algorithm is obvious, with the estimate depth able to fit the real depth. The scatterplot also describes that bottom types with high mean reflectance (bright bottom types) tend to produce less error, whereas bottom types with low mean reflectance (dark bottom types) shows range of errors.

The differences between the real and estimated depth values were defined as residuals and are summarized in Table 3. The maximum residual was ~1 m and the RMS residual was less than 0.4 m. In varying water quality and bottom-type conditions of 137

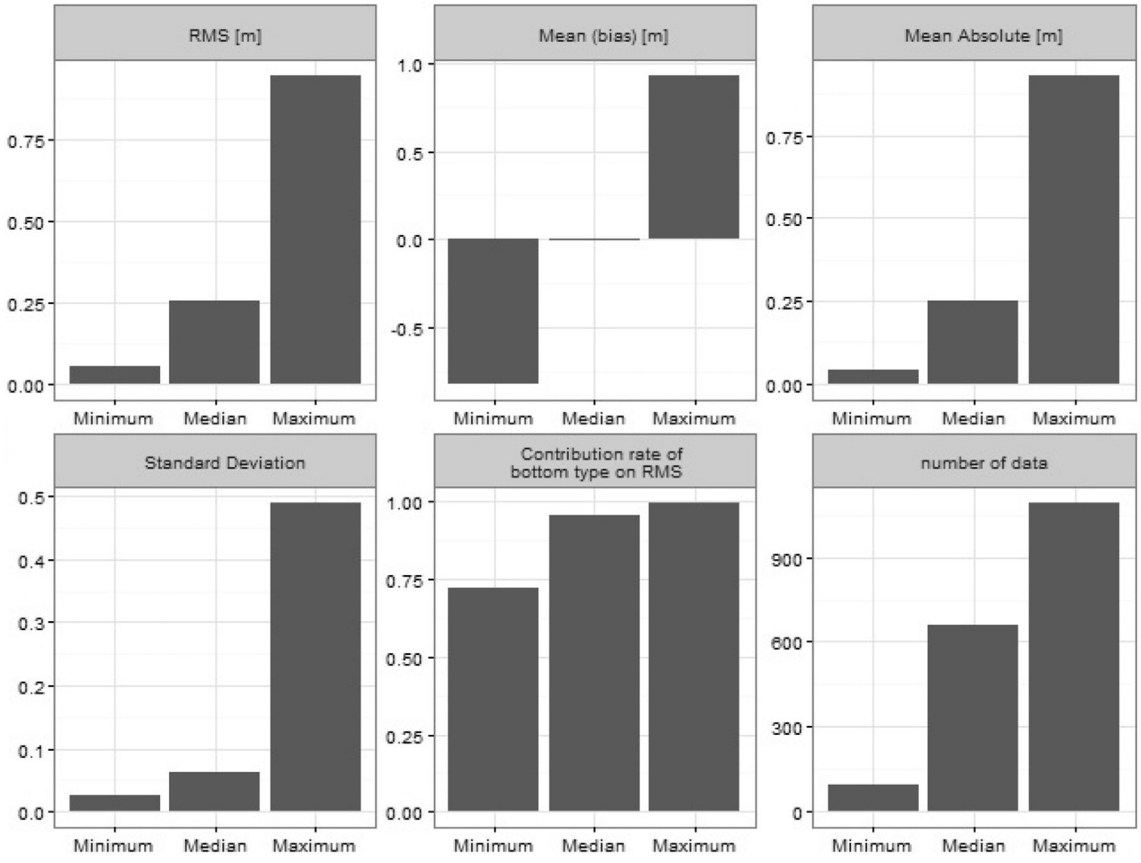

Fig. 3. Estimated depth residuals for each bottom type.

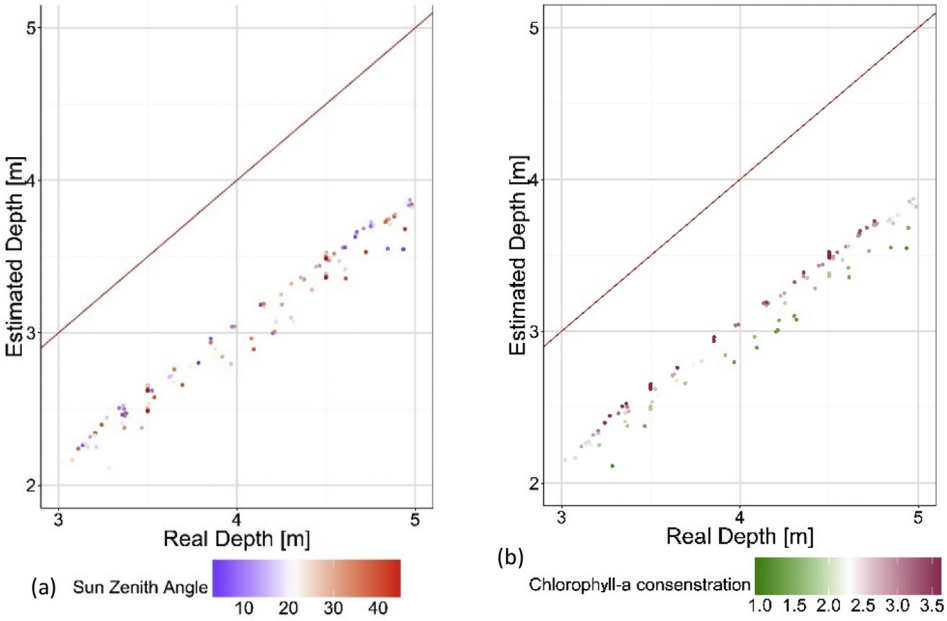

Fig. 4. Scatter plot of the estimated versus real depths for bottom type ID "b155Encrusting20 ms," which exhibited the highest RMS error residual value (0.95117 m). The plots are color-coded by (a) solar zenith angle (degrees) and (b) chlorophyll-a concentration (mg/m^3). The red line is y = x. (For interpretation of the references to colour in this figure legend, the reader is referred to the web version of this article.)

different spectra, Lyzenga's multispectral bathymetry model achieved good depth estimation accuracy. This result supports the generality of Lyzenga's multispectral bathymetry model under this wide range of optical conditions and numbers of bottom types.

This finding on the generality of Lyzenga's multispectral bathymetry appears to be well-supported by previous studies, in which the application of Lyzenga's formula on real coastal environment images acceptably estimates water depth (Liceaga-Correa and Euan-Avila, 2002; Pacheco et al., 2015; Vinayaraj et al., 2016; Manessa et al., 2016a). The accuracies achieved in previous studies are 0.78 m–0.88 m and 0.8 m–2.63 m for R^2 and RMS error, respectively. The accuracy of real images is far higher that of the simulation-based analysis (Table 3), as the optical conditions and bottom types are less varied. The resistance parameters, (i.e., image spatial and spectral resolution, image noise, data quality, and site dependency) contribute significantly to the accuracy achieved in real-image analysis; however, in this study, resistance parameters were excluded, as the simulated dataset is assumed to be zero-noise. Thus, these resistance parameters could well be responsible for several failures (Stumpf et al., 2003; Manessa et al., 2016a) in applying Lyzenga's formula to real images.

3.2.2. Relationship between accuracy and optical condition

Since the simulated dataset was free of noise, the average of the estimated depth residuals equaled zero. Thus, as Deakin and Kildea (1999) explain, RMS error can be broken up, as

$$RMS^2 = \left(\frac{1}{n}\sum_i (r_i - \bar{r}_i)^2\right) + \left(\bar{r}_i - r_i\right)^2 \quad (29)$$

that is,

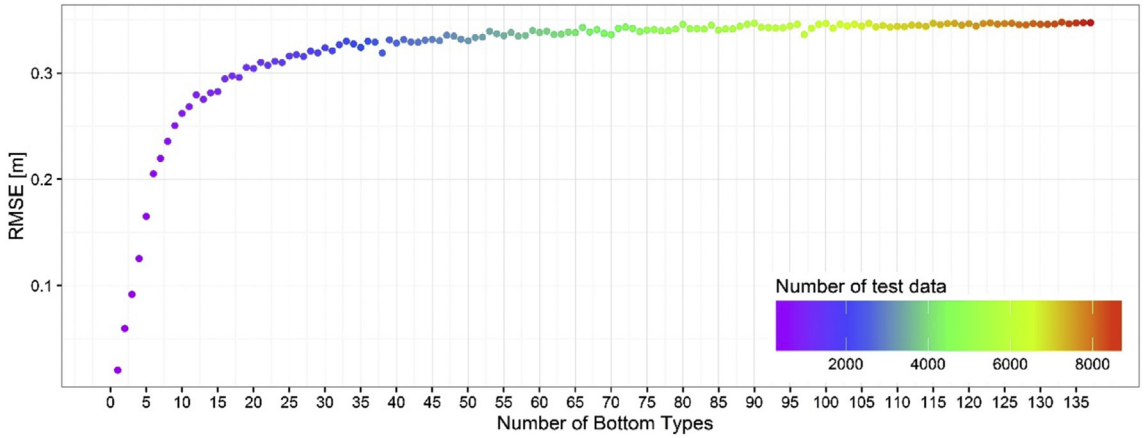

Fig. 5. RMS error of depth estimation from 100-sample cross-validation of each instance of bottom type quantity.

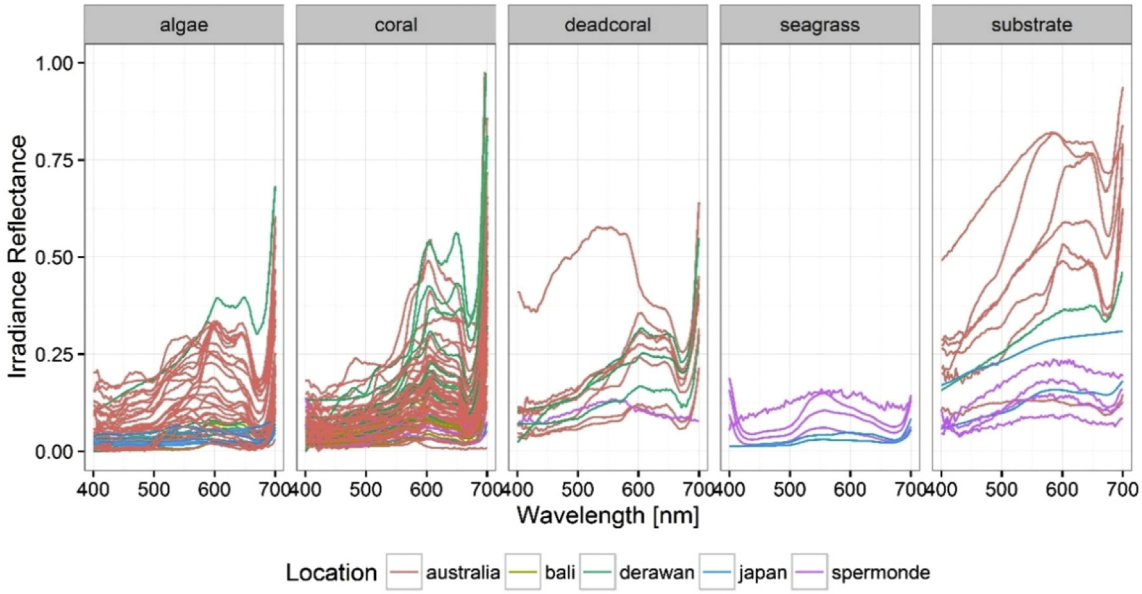

Fig. 6. 165 bottom-type spectra measured in coral reef environments for five bottom-cover classes. Line color denotes the measurement location, as defined in the legend. (For interpretation of the references to colour in this figure legend, the reader is referred to the web version of this article.)

$$RMS^2 = \textit{estimate of standard deviation} + (\textit{estimate of bias})^2$$

The mean component of the RMS error corresponds to the bias caused by the bottom type, whereas the standard deviation component corresponds to the error caused by other optical conditions (depth, chlorophyll-a concentration, and solar zenith angle). It follows that the contribution rate of the bottom type to the RMS error is calculated by:

$$\textit{contribution rate of bottom types on RMS} = \textit{mean absolute}\ /RMS \quad (30)$$

Fig. 3 shows the minimum, median, and maximum summary statistics for each bottom type and the contribution rate of the bottom type to the RMS error. First, the results show that for any bottom type, the RMS error was less than 1 m. Second, the residuals were dominated by bottom-type effects (Fig. 3), whereas water depth, solar zenith angle, and chlorophyll concentration contributed to the residuals to a lesser degree (a maximum of 18%). An additional indication of bottom types contributing highly to the RMS error is that 98 of 137 bottom samples provided a bottom type contribution rate greater than 0.9 to the RMS error. Moreover, Fig. 4 shows that, for the bottom type with the highest RMS error (ID "b155Encrusting20 ms"), the effect of chlorophyll-a concentration and solar zenith angle on RMS error was only 0.17 m, far smaller than the 1-m effect of bottom type. Since the majority of the RMS error of the residuals from the depth estimation was distributed close to the parity line, bottom type had the greatest influence of all variables on RMS error. Lastly, Fig. 4 also shows that chlorophyll-a concentration affects accuracy more than sun zenith angle. In fact, the lower the chlorophyll-a concentration was, the less error occurred in estimation depth.

3.3. Effect of the number of bottom types on depth estimation accuracy

Fig. 5 presents the performance of Lyzenga's multispectral bathymetry model under varied bottom-type conditions. The RMS error of bathymetry estimation increased with the number of bottom types. The model performed best on the uniform distribution (one bottom type), with an RMS error of 0.02 m (Fig. 5); RMS error increased significantly with each additional bottom type. This increase in error decreased significantly after approximately 15 bottom types and plateaued at around 30 bottom types; at high bottom-type diversity, there was a high probability of a bottom type with similar spectral properties being added to the group of bottom types. As shown in Fig. 6, many bottom types had very

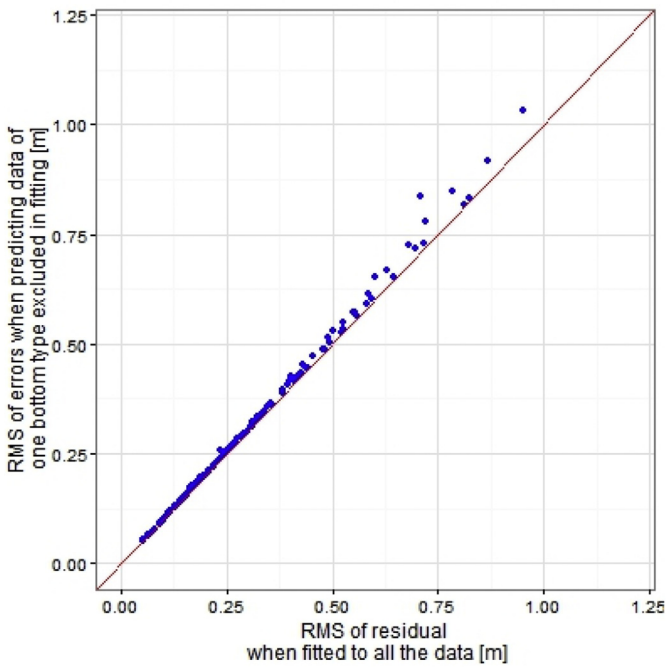

Fig. 7. Scatter plot of RMS residuals when all bottom types were used in fitting versus RMS error when one bottom type was excluded. Each point represents a bottom type. The red line is y = x. (For interpretation of the references to colour in this figure legend, the reader is referred to the web version of this article.)

Table 4
RMS residual statistics of the estimated depth of each bottom type using all bottom-type data and without the estimated bottom type.

	Minimum	Median	Maximum
RMS when all bottom types are used in training (A) [m]	0.05	0.26	0.95
RMS when one bottom type is excluded from training (B) [m]	0.05	0.26	1.03
Incensement Ratio of RMS rate of error (B/A - 1)	0.001	0.02	0.2
Increase value of RMS (B − A) [m]	0.00005	0.004	0.13

similar spectral characteristics.

These results offer unprecedented evidence for the use of Lyzenga's formula for diverse coral reef environments. Doubts about the performance of Lyzenga's method for diverse bottom types (Stumpf, 2003; Su et al., 2013) and for cases with more bottom types than bands (Lyzenga et al., 2006) were not proven. However, it is natural that less diverse bottom types lead to better estimation accuracy than more diverse bottom types.

3.4. Lyzenga's method for water depth estimation with unknown bottom types

Fig. 7 compares the RMS residuals when all bottom types were used in fitting and the RMS error when one bottom type was excluded from fitting; the plotted point falls closet to the line $y = x$. Moreover, removing of the bottom type from fitting increased the error but not significantly. This result shows that the model can predict the water depth of an unknown bottom type almost as accurately as for a known bottom type.

Table 4 shows statistics of the residuals of water depth estimation for each bottom type in cases in which all bottom types were known and in which the tested bottom type was excluded from the calibration of the estimation model. The incensement rate of error for the tested or unknown bottom type was excluded from model calibration. It is interesting to note that the maximum RMS residual when the bottom type was excluded was 1.03 m, which is just 0.08 m higher than if all bottom types were used (RMS residual = 0.95 m).

This result confirmed that our water-depth estimation model was general enough to predict water depth from a coral reef area with unknown bottom types. However, careful attention must be paid to bottom type diversity in the model prediction input. Excluding one bottom type of 134 still made the input (simulated dataset of 133 bottom types) diverse enough for model prediction; the depth of the excluded bottom type could still be estimated accurately. These results point to the likelihood that Lyzenga's formula can estimate the depth of an unknown bottom type because the known depth used as input for building the model has a bottom type that represents (or is similar to) the unknown bottom type. Further studies that consider realistic cases, such as less diverse bottom types, as input need to be performed.

4. Conclusions

In this study, a WorldView-2 above-water remote sensing reflectance dataset was simulated for Case-1 waters of a coral reef environment. The simulation dataset was used to verify the generality of the multispectral bathymetry model from Lyzenga et al. (2006) under varying bottom type, solar zenith angle, and water quality (represented by chlorophyll-a concentration) conditions. First, for a wide range of bottom types and variable optical conditions (solar zenith angles and chlorophyll-a concentrations), Lyzenga's multispectral bathymetry model was sufficiently general to accurately estimate water depth. Lyzenga et al. (2006) noted that the application of this method was limited to cases in which the number of bottom types is no greater than the number of multispectral bands. Surprisingly, the results of this study contradict the previous result; the simulation-based analysis shows that this model still works well ($R^2 = 0.97$ and RMS residual 0.4 m) for 137 bottom types, which is much greater than the number of multispectral bands used (5 visible bands of WorldView-2 images). Second, bottom type diversity dominantly influenced the performance of Lyzenga's multispectral bathymetry model (72–99% contribution to RMS residual), whereas other optical conditions made only minor contributions (maximum 18% contribution to RMS residual). Third, Lyzenga's depth estimation accuracy became poorer with the cumulative increase in the number of bottom types. Interestingly, beyond a certain number of bottom types (~30), the change in accuracy plateaued for any increase in bottom type number. Lastly, the depth of an unknown bottom type can be predicted accurately (~0.13 m RMS residual incensement) if the prediction model is built using diverse bottom type conditions (133 bottom types).

This study provides a basis for other research efforts using Lyzenga's multispectral bathymetry to map shallow coral reef bathymetry. However, it should be noted that this promising result was performed under a zero-noise assumption. In reality, multispectral imagery contains noise—especially in the shorter wavelength bands—due to Rayleigh scattering. Thus, further studies that consider the contribution of noise must be performed.

Acknowledgments

M.D.M. Manessa acknowledges support from the Indonesia Endowment Fund for Education (LPDP) by the Ministry of Finance for the doctoral scholarship. We are very grateful to M. Nurlidiasari, C.M. Roelfsema, S.R. Phinn, and E.J. Hochberg, who provided their coral reef bottom spectral measurement data to be used in this study. This research was partially supported by a research grant from the Kurita Water and Environment Foundation (No. 15B013).

Appendix. IOP model

We used the IOP model for Case-1 waters, which has been described in publications addressing absorption and scattering (Bricaud et al., 1998; Morel and Maritorena, 2001; Morel et al., 2002). The model is characterized as follows:

$$a_p(z,\lambda) = A(\lambda)[Chl(z)]^{E(\lambda)} \quad \text{(A.1)}$$

$$a_y(z,\lambda) = a_p(z,\lambda_{440})e^{[-0.0162(\lambda-\lambda_{440})]} \quad \text{(A.2)}$$

$$b_{bp}(z,\lambda) = \breve{B}_p(z,\lambda)b_p(z,\lambda) \quad \text{(A.3)}$$

$$\breve{B}_p(z,\lambda) = \ 0.002 + (0.01[0.5 - 0.25\log_{10}(Chl(z))]) \quad \text{(A.4)}$$

$$b_p(z,\lambda) = c_p(z,\lambda) - a_p(z,\lambda) \quad \text{(A.5)}$$

$$c_p(z,\lambda) = 0.407\ [Chl(z)]^{0.795}(\lambda/660)^{v} \quad \text{(A.6)}$$

$$v = 0.5[log10Chl(z) - 0.3]\ for\ 0.02 < Chl(z) < 2$$

$$= 0\ for\ Chl(z) > 2$$

where A and E are numerical constants (Bricaud et al., 1998); $Chl(z)$ is the Chlorophyll-a concentration in mgm^3; a_p and a_y are absorption coefficients for chlorophyll-bearing particles and covarying yellow matter (CDOM); and b_{bp} and b_p are the particle phase functions and particle backscatter fraction, respectively.

References

Baker, K.S., Smith, R.C., 1982. Bio-optical classification and model of natural waters. 2. Limnol. Oceanogr. 27 (3), 500–509. https://doi.org/10.4319/lo.1982.27.3.0500.

Bricaud, A., Morel, A., Babin, M., Allali, K., Claustre, H., 1998. Variations of light absorption by suspended particles with chlorophyll *a* concentration in oceanic (Case-1) waters: analysis and implications for bio-optical models. J. Geophys. Res. 103 (C13), 31033–31044. https://doi.org/10.1029/98JC02712.

Carder, K.L., Cannizzaro, J.P., Lee, Z., 2005. Ocean color algorithms in optically shallow waters: limitations and improvements. Proc. SPIE 5885, 588506. https://doi.org/10.1117/12.615039.

Clark, R.K., Fay, T.H., Walker, C.L., 1987. Bathymetry calculations with Landsat 4 TM imagery under a generalized ratio assumption. Appl. Opt. 26 (19), 4036–4038. https://doi.org/10.1364/AO.26.4036_1.

Daniell, J.J., 2008. Development of a bathymetric grid for the Gulf of Papua and adjacent areas: a note describing its development. J. Geophys. Res. Earth Surf. 113 (F1) https://doi.org/10.1029/2006JF000673.

Deakin, R.E., Kildea, D.G., 1999. A note on standard deviation and RMS. Aust. Surv. 44 (1), 74–79.

Eugenio, F., Marcello, J., Martin, J., 2015. High-resolution maps of bathymetry and benthic habitats in shallow-water environments using multispectral remote sensing imagery. IEEE Trans. Geoscience Remote Sens. 53 (7), 3539–3549. https://doi.org/10.1109/TGRS.2014.2377300.

Flener, C., Lotsari, E., Alho, P., Käyhkö, J., 2012. Comparison of empirical and theoretical remote sensing based bathymetry models in river environments. River Res. Appl. 28 (1), 118–133. https://doi.org/10.1002/rra.1441.

Hochberg, E.J., Atkinson, M.J., Apprill, A., Andréfouët, S., 2004. Spectral reflectance of coral. Coral Reefs 23 (1), 84–95. https://doi.org/10.1007/s00338-003-0350-1.

Jupp, D.L.B., 1988. Background and extensions to depth of penetration (DOP) mapping in shallow coastal waters. In: Proceedings of the Symposium on Remote Sensing of the Coastal Zone. September1988, Gold Coast, Queensland, Australia, pp. IV.2.1–IV.2.19.

Kabiri, K., 2017. Accuracy assessment of near-shore bathymetry information retrieved from Landsat-8 imagery. Earth Sci. Informatics 10 (2), 235–245. https://doi.org/10.1007/s12145-017-0293-7.

Kanno, A., Tanaka, Y., 2011. Modified Lyzenga's method for estimating generalizes coefficients of satellite-based prediction of shallow water depth. IEEE Geoscience Remote Sens. Lett. 9 (4), 715–719. https://doi.org/10.1109/LGRS.2010.2051658.

Kanno, A., Tanaka, Y., Kurosawa, A., Sekine, M., 2013. Generalized Lyzenga's predictor of shallow water depth for multispectral satellite imagery. Marine Geodesy 36 (4), 365–376. https://doi.org/10.1080/01490419.2013.839974.

Leckie, D.G., Cloney, E.E., Jay, C., Paradine, D., 2005. Automated mapping of stream features with high-resolution multi-spectral imagery: an example of the capabilities. Photogrammetric Eng. Remote Sens. 71 (2), 145–155.

Lee, Z., Carder, K.L., Mobley, C.D., Steward, R.G., Patch, J.S., 1999. Hyperspectral remote sensing for shallow waters: 2. Deriving bottom depths and water properties by optimization. Appl. Opt. 38 (18), 3831–3943. https://doi.org/10.1364/AO.38.003831.

Lee, Z., Weidemann, A., Arnone, R., 2013. Combined Effect of reduced band number and increased bandwidth on shallow water remote sensing: the case of worldview 2. IEEE Trans. Geoscience Remote Sens. 51 (5), 2577–2586.

Liceaga-Correa, M.A., Euan-Avila, J.I., 2002. Assessment of coral reef bathymetric mapping using visible Landsat Thematic Mapper data. Int. J. Remote Sens. 23 (1), 3–14. https://doi.org/10.1080/01431160010008573.

Lyzenga, D.R., 1978. Passive remote sensing techniques for mapping water depth and bottom features. Appl. Opt. 17 (3), 379–383.

Lyzenga, D.R., 1985. Shallow-water bathymetry using combined lidar and passive multispectral scanner data. Int. J. Remote Sensening 6 (1), 115–125, 0.1080/01431168508948428.

Lyzenga, D.R., Malinas, N.P., Tanis, F.J., 2006. Multispectral bathymetry using a simple physically based algorithm. IEEE Trans. Geoscience Remote Sens. 44 (8), 2251–2259. https://doi.org/10.1109/TGRS.2006.872909.

Manessa, M.D.M., Kanno, A., Sekine, M., Ampou, E.E., Widagti, N., As-syakur, A.R., 2014. Shallow-water benthic identification using multispectral satellite imagery: investigation on the effects of improving noise correction method and spectral cover. Remote Sens. 6 (5), 4454–4472. https://doi.org/10.3390/rs6054454.

Manessa, M.D.M., Kanno, A., Sekine, M., Haidar, M., Yamamoto, K., Imai, T., Higuchi, T., 2016a. Satellite-derived bathymetry using random forest algorithm and Worldview-2 imagery. Geoplanning J. Geomatics Plan. 3 (2), 117–126. https://doi.org/10.14710/geoplanning.3.2.117-126.

Manessa, M.D.M., Kanno, A., Sekine, M., Haidar, M., Nurdin, N., 2016b. Lyzenga multispectral bathymetry formula for Indonesian shallow coral reef: evaluation and proposed generalized coefficient. Proc. SPIE. https://doi.org/10.1117/12.2240550, 999900-999900.

Manessa, M.D.M., Haidar, M., Budhiman, S., Winarso, G., Kanno, A., Sagawa, T., Sekine, M., 2016c. Evaluating the performance of Lyzenga's water column correction in case-1 coral reef water using a simulated Wolrdview-2 imagery. Proc. IOP Conf. Ser. Earth Environ. Sci. 47 (1), 012018. https://doi.org/10.1088/1755-1315/47/1/012018.

Morel, A., Maritorena, S., 2001. Bio-optical properties of oceanic waters: a reappraisal. J. Geophys. Res. 106 (C4), 7163–7180. https://doi.org/10.1029/2000JC000319.

Morel, A., Antoine, D., Gentili, B., 2002. Bidirectional reflectance of oceanic waters: accounting for Raman emission and varying particle scattering phase function. Appl. Opt. 41 (30), 6289–6306. https://doi.org/10.1364/AO.41.006289.

Nurlidiasari, M., 2004. The Application of QuickBird and Multi-temporal Landsat TM Data for Coral Reef Habitat Mapping (M.S. Thesis). ITC, Enschede, the Netherland.

Pacheco, A., Horta, J., Loureiro, C., Ferreira, Ó., 2015. Retrieval of nearshore bathymetry from Landsat 8 images: a tool for coastal monitoring in shallow waters. Remote Sens. Environ. 159, 102–116. https://doi.org/10.1016/j.rse.2014.12.004.

Paredes, J.M., Spero, R.E., 1983. Water depth mapping from passive remote-sensing data under a generalized ratio assumption. Appl. Opt. 22 (8), 1134–1135. https://doi.org/10.1364/AO.22.001134.

Philpot, W.D., 1989. Bathymetric mapping with passive multispectral imagery. Appl. Opt. 28 (8), 1569–1578. https://doi.org/10.1364/AO.28.001569.

Ribeiro, S.R.A., Centeno, J.A.S., Krueger, C.P., 2008. An estimate of depth from a bathymetric survey and IKONOS II data by means of artificial neural network. Bol. Ciências Geodésicas 14, 171–185.

Roelfsema, C.M., Phinn, S.R., 2012. Spectral reflectance library of selected biotic and abiotic coral reef features in heron reef. (Pangaea, bremerhaven, Germany). https://doi.org/10.1594/PANGAEA.804589 online, dataset.

Sagawa, T., Boisnier, E., Komatsu, T., Mustapha, K.B., Hattour, A., Kosaka, N., Miyazaki, S., 2010. Using bottom surface reflectance to map coastal marine areas: a new application method for Lyzenga's model. Int. J. Remote Sens. 31 (12), 3051–3064. https://doi.org/10.1080/01431160903154341.

Sagawa, T., Mikami, A., Aoki, M.N., Komatsu, T., 2012. Mapping seaweed forests with IKONOS image based on bottom surface reflectance. Proc. SPIE 8525, 85250Q. https://doi.org/10.1117/12.975678.

Spitzer, D., Dirks, R.W.J., 1987. Bottom influence on the reflectance of the sea. Int. J. Remote Sens. 8 (3), 279–290. https://doi.org/10.1080/01431168708948642.

Stumpf, R.P., Holderied, K., Sinclair, M., 2003. Determination of water depth with high-resolution satellite imagery over variable bottom types. Limnol. Oceanogr. 48 (1), 547–556. https://doi.org/10.4319/lo.2003.48.1_part_2.0547.

Su, H., Liu, H., Heyman, W.D., 2008. Automated derivation of bathymetric information from multi-spectral satellite imagery using a non-linear inversion model. Mar. Geod. 31 (4), 281–298. https://doi.org/10.1080/01490410802466652.

Su, H., Liu, H., Wang, L., Filippi, A.M., Heyman, W.D., Beck, R.A., 2013. Geographically adaptive inversion model for improving bathymetric retrieval from satellite multispectral imagery. IEEE Trans. Geoscience Remote Sens. 52 (1), 465–476. https://doi.org/10.1109/TGRS.2013.2241772.

Vinayaraj, P., Raghavan, V., Masumoto, S., 2016. Satellite-derived bathymetry using adaptive geographically weighted regression model. Mar. Geod. 39 (6), 458–478. https://doi.org/10.1080/01490419.2016.1245227.

Yuzugullu, O., Aksoy, A., 2014. Generation of the bathymetry of a eutrophic shallow lake using WorldView-2 imagery. J. Hydroinformatics 16 (1), 50–59. https://doi.org/10.2166/hydro.2013.133.